Journal of Power Sources 498 (2021) 229908

Contents lists available at ScienceDirect

Journal of Power Sources

journal homepage: www.elsevier.com/locate/jpowsour

The functional separator for lithium-ion batteries based on phosphonate modified nano-scale silica ceramic particles

Boyang Huang [a], Haiming Hua [a], Longqing Peng [a], Xin Wang [a], Xiu Shen [a], Ruiyang Li [a], Peng Zhang [b,**], Jinbao Zhao [a,*]

[a] State Key Laboratory of Physical Chemistry of Solid Surfaces, Collaborative Innovation Centre of Chemistry for Energy Materials, State-Province Joint Engineering Laboratory of Power Source Technology for New Energy Vehicle, Engineering Research Center of Electrochemical Technology, Ministry of Education, College of Chemistry and Chemical Engineering, Xiamen University, Xiamen, 361005, PR China

[b] College of Energy & School of Energy Research, Xiamen University, Xiamen, 361102, China

HIGHLIGHTS

- Flame retardant phosphonate is fixed on silica ceramic by double bond polymerization.
- Immobilized phosphonate will not be embedded in the graphite anode in battery cycles.
- Phosphonate further enhances thermal stability of functional separator.
- Accordingly, flame resistances of separator itself and cells are markedly improved.

ARTICLE INFO

Keywords:
Phosphonate additive
Ceramic separator
Lithium-ion batteries
Thermal stability
Flame resistance
Immobilization

ABSTRACT

In lithium-ion batteries (LIBs), benefiting from various functional components, functional separators can possess different capabilities to cope with the risks in complex application scenarios. In this work, a functional separator based on the phosphonate-modified nano-scale silica ceramic particles is fabricated to reduce the safety risks in LIBs. Through an anhydrous polymerization process, dimethyl vinylphosphonate (DMVP), a kind of widely used flame retardants, is grafted on silica (SiO_2). Then the modified SiO_2 ($mSiO_2$) is coated on the pristine polyethylene separator by a typical coating process. Combining the function of the ceramic and phosphonate, the modified ceramic separator displays substantially enhanced thermal stability, without visual thermal shrink up to 200 °C. The flame resistances of separator itself and pouch cells are also significantly improved, even though flammable electrolyte is added. Different from the case when the phosphonate is used as an additive in electrolyte, the phosphonate is fixed firmly on the separator and not easy to be embedded in carbon anode after battery cycles. The coin cells assembled with the modified separators are away from the irreversible loss of discharge capacity and low Coulombic efficiency for the first cycle, which can be attributed to the firm immobilization of organic phosphonate.

1. Introduction

Nowadays, lithium-ion batteries (LIBs) not only have been widely used in portable electronic devices (mobile phone, laptop, camera, etc.) [1,2], but also have become one of the most promising energy storage systems (ESSs) for the large-scale application (electric vehicle, smart grid, etc.) [3], owing to their advantages of high energy density, excellent cycle life and low self-discharging. However, there still exist lots of problems in the practical large-scale applications, especially the safety issues, which would cause fires or even explosions due to the large amount of energy stored in the system [4–6].

Taking a look at the structure of LIBs, a typical LIB cell consists of a cathode electrode, an anode electrode, electrolyte and a separator. In a cell construction, a separator plays a vital role for the electrochemical and safety performance, because it divides the cathode electrode from the anode electrode with only allowing the ion transport in electrolyte

* Corresponding author.
** Corresponding author.
E-mail addresses: pengzhang@xmu.edu.cn (P. Zhang), jbzhao@xmu.edu.cn (J. Zhao).

https://doi.org/10.1016/j.jpowsour.2021.229908
Received 28 January 2021; Received in revised form 28 March 2021; Accepted 7 April 2021
Available online 30 April 2021

[7,8]. At present, separators based on microporous polyolefin membranes including polyethylene (PE) and polypropylene (PP) are very common in commercial LIBs due to its excellent chemical stability and mechanical strength as well as the mature and steady production engineering. But there are still some disadvantages not to be ignored. At elevated temperatures, polyolefin membranes could not provide good mechanical strength anymore because of thermal shrinkage. Additionally, polyolefin material always could not be wetted well by commercial organic electrolyte. The former one means there would be an unexpected internal short circuit after an unexpected heat generation in LIB, which could cause thermal runaway with an ignition, even an exploration, while the later one might bring with a decrease of electrolyte absorption and a lower ionic conductivity, which could be harmful to both capacity retention and power capability [9,10].

To solve the above problems, many efforts have been made by researchers. For example, since the flammability of solid and gel states is lower than that of liquid, there are many related works in the fields of solid polymer electrolyte (SPE) and gel polymer electrolyte (GPE) [11–15]. However, intrinsic properties of solid and gel state limit the ionic conductivity and mechanical strength, respectively. For SPEs, the ionic conductivity of dry polymer membranes, especially low ionic conductivity at room temperature, is a barrier of lithium ion transfer between solid phases. As for GPEs, it is usually difficult to maintain a certain shape under actual working conditions for a gel phase [16,17]. At present, the modification of the commercial polyolefin separators is still thought to be the most practical way to overcome the problems mentioned above. For example, the inorganic ceramics (Al_2O_3 and SiO_2) are coated on the surface of commercial PE and PP separator to develop the ceramic separator, which is regarded to be an effective strategy and has been extended to practical application [18–20].

For the development of ceramic coated separator, the strategies could be roughly divided into three categories, including the introduction of functional components, the structure design and the preparation methods. These three strategies are not independent of each other, in fact, they are interrelated, including but not limited to the fact that the proper preparation method can be used to prepare the corresponding functional components and the appropriate structure strategy is conducive to the function of the components. In a specific research process, these three factors must be considered, but one of them will be emphasized in the research process. In terms of functional components, both organic and inorganic substances are available based on its different features. In general, an inorganic ceramic component such as $Li_{6.4}La_3Zr_{1.4}Ta_{0.6}O_{12}$ (LLZTO) could provide better conduction properties [21], and an organic component could improve the interface contact and adhesion. For example, dopamine is proved to be helpful to construct adhesion site [22], and cellulose rich in reactive groups can improve the wettability of the diaphragm and ensure the cohesiveness [23]. For the aspect of structural strategies, the most common strategy is building a multi-layer coating [24]. Combined with some specific preparation methods, specific structures such as textile structures [25], sandwich structures [26], and filling structures [27] can be synthesized. Besides, it is possible to adjust the pores of the separator to form a specific anisotropic shape to improve liquid absorption [28]. As for the preparation methods, in addition to the most common slurry coating process, industrial coating methods such as dip coating are also be used [26]. In addition, some novel approaches such as atomic layer deposition (ALD) [29] and micro-vacuum coating [30] also have certain applications in the preparation of functional ceramic layers.

In previous functional ceramic coated separator work of our group, for structural components, we have used poly (methyl methacrylate) (PMMA) [31], polyimide (PI) [32], polydopamine (PDA) [33], phenol-formaldehyde resin (PFR) and ammonium polyphosphate (APP) [34–36]; for structural strategies, we have proposed multi-layer composite and core-shell structure; for preparation methods, we have used ceramic coating and atomic layer deposition (ALD) [37]. These researches make it possible to introduce different component materials with different functions through rational ceramic structural design to develop a multi-functional ceramic coating separator rather than a single functional membrane. Besides, mentioned in our previous work, the most important safety issue caused casualties is the drastic burning of combustible materials in LIBs [35]. In order to prevent the combustion in LIBs, reducing the flammability of battery materials is the most direct method. And for separators, it is possible to introduce flame-retardant functional components to achieve this purpose. Considering our research foundation of preparing modified ceramic particles, constructing different ceramic layers and designing constructions with heat-resistant components, it seems worthwhile to modify a refractory component directly on the ceramic particles to obtain better thermal performances of a functional ceramic coated separator.

As a suitable heat-resistant component, we have turned our attention to electrolyte additives. These additives are functional chemicals that are added to the electrolyte in a limited amount to enhance specific performance such as preventing overcharge, optimizing the generation of solid electrolyte interphase, improving low temperature performance and so on [38–40]. Among electrolyte additives, flame retardants, including fluorinated organic solvent, organic phosphonate, organic borate and silane, are helpful to a less flammability [41,42]. Therein, it has been proved that phosphorus free radicals released by organic phosphonate after heating could react with hydrogen free radicals to block the chain reaction of hydrogen free radicals and oxygen free radicals. In addition to this reasonable gas phase flame retardant theory, the condensed phase (phosphate generated during the decomposition of organic phosphonates) is also considered as an auxiliary means in the flame retardant process. What's more, organic phosphonate itself has low toxicity, and there is no toxic chemical generated in the flame-resisting process. So various kinds of organic phosphonate were widely researched, and it was found that even simple phosphonate such as trimethyl phosphate is helpful to reduce flammability of electrolyte in LIBs [43–45]. However, the reaction of organic phosphonate and commercial graphite anode would make phosphonate embedded into anode electrode, thus influencing the sheet structure of graphite and causing an irreversible loss of capacity [46,47].

In this study, an organic-inorganic hybrid ceramic material which has both advantages of organic phosphonate and inorganic ceramics, similar to other kinds of hybrid layers [48], was applied as coating layer to develop a bifunctional ceramic coated separator with both flame resistant and heat resistant. As the schematic illustration shown in Fig. 1, 3-Methacryloxypropyltrimethoxysilane (KH570) modified SiO_2 was firstly synthesized by a reverse microemulsion method [49]. Then in an anhydrous nitrogen atmosphere built by Schlenk line, dimethyl vinylphosphonate (DMVP) reacted with KH570, where the double bond polymerization of KH570 and DMVP happened to obtain the DMVP-grafted SiO_2 particles. Afterwards, a typical coating process was utilized on the grafted particles and commercial PE separator (manufactured by a wet process) to produce phosphonate-ceramic composite modified polyolefin membranes [50]. Through the structural and thermal characterization, the thermal stability of the modified separator was found to be significantly enhanced. The rate capability and cycling performance of the batteries, in which the ceramic side of the separator faced to the cathode, suggested that grafted DMVP did not affect electrochemical performance, whether in any kind of half cells assembled. This study suggests that it is feasible to combine a kind of electrolyte additives with separator to utilize its advantages and avoid some adverse effects, and it would be a good strategy to find other electrolyte additives as the possible modifiers of modified separators.

2. Experimental section

2.1. Synthesis of modified SiO_2 particles

KH570 modified SiO_2 particles were prepared in reverse microemulsions formed by Brij-58/cyclohexane/water. 6.74 g of

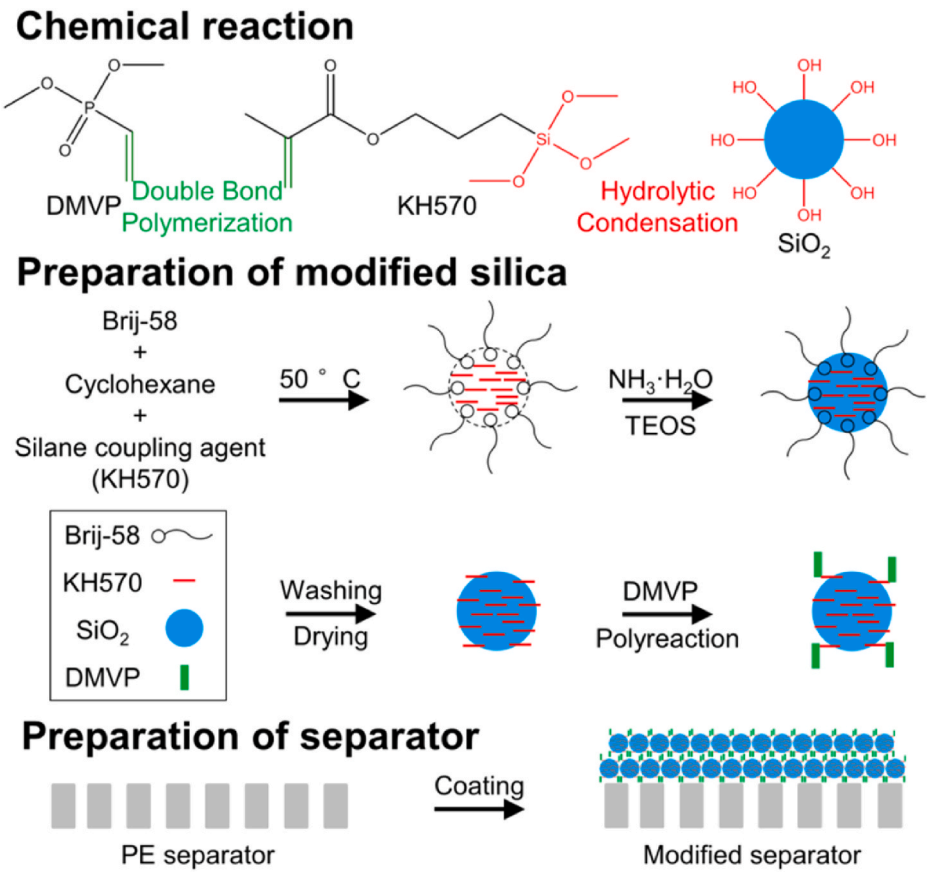

Fig. 1. Schematic illustration of the preparing process of modified silica particles and modified separators.

Polyoxyethylene (20) cetyl ether (Brij-58, Shanghai Aladdin Bio-Chem Technology Co., Ltd.) was added to a 100 mL flask containing 15 mL of cyclohexane, and the flask was heated to 50 °C with stirring to make the solution well mixed. 0.3 mL of KH570 (Zhangjiagang Guotaihuarong New Chemical Materials Co., Ltd) was added to the flask and then a reverse microemulsion system was formed. After 1 h of stirring, 2.4 mL of ammonium hydroxide was added to the system drop by drop; after next 0.5 h of stirring, 2 g of tetraethyl orthosilicate (TEOS, AR, Sinopharm Chemical Reagent Co., Ltd.) was added in the same way and SiO_2 modification process started immediately. 2 h later the generation process went well, and 15 mL of isopropanol was added to stop the process and demulsificate the microemulsion. Waiting for 5 min of ultrasonication, the mixture was put into the centrifuge set at 6000 rpm for 10 min, after which the precipitate was scraped, washed by isopropanol twice and dried at 100 °C for 24 h to gain the dry product [49].

Then dimethyl vinylphosphonate (DMVP, 98%, Strem Chemicals, Inc.) grafted SiO_2 particles ($mSiO_2$) were prepared through polymerization reaction of DMVP and KH570 modified SiO_2 particles in a Schlenk line free from water and oxygen. In the case, standard Schlenk line techniques under dry nitrogen was used and all reagents such as toluene, 2, 2-azobisisobutyronitrile (AIBN) and DMVP were pretreated by 4A-type molecular sieves to remove the water. 0.30 g of KH570 modified SiO_2 particles was suspended in 30 mL of toluene with stirring, then 0.01 g of AIBN (about 0.5 wt % of reactant weight, as initiator) and 1.5 mL of DMVP were added. After 3 repeats of vacuuming and purging nitrogen for 30 min per purge, the system was at low water and oxygen levels and then heated to 70 °C with stirring to initiate the polymerization reaction and cooled with ice water 24 h later to stop that reaction. After centrifuging at 6000 rpm for 10 min, the precipitate was washed by toluene twice and dried at 100 °C for 24 h.

2.2. Preparation of the ceramic coating separators

The slurry for ceramic-coating layer was prepared by mixing modified SiO_2 particles and poly (vinylidene fluoride) (PVDF) into N, N-dimethylformamide (DMF) solvent, where the weight of modified SiO_2 particles/PVDF/DMF was fixed at 0.7 g/0.3 g/5 g. After ultrasonicated for 10 min, the slurry was subjected to vigorous mixing with a speed of 400 rpm for 10 h. A PE separator manufactured by a wet process (Asahi Kasei Corp.) was selected to be the substrate, and the slurry was applied to one side of the pristine PE separator using an automatic film-coating machine. The modified SiO_2 coated PE separator was dried on a 60 °C plate for 4 h, and then additionally dried under Schlenk line at 60 °C for 12 h to remove the solvent. In the same method, normal SiO_2 coated PE separator could be prepared by using normal SiO_2 particles instead of modified SiO_2 particles [50].

2.3. Electrode preparation and cell assembly

NMP-based slurry was prepared by mixing 1.08 g $LiFePO_4$ cathode powder (LFP, Guoxuan High-Tech Co., Ltd.), 0.06 g acetylene black and 0.06 g PVDF into appropriate amount of N-methyl-2-pyrrolidone (NMP) solvent and stirring. Then a piece of aluminium foil was chosen to be coated by the slurry and dried at 80 °C for 12 h to prepare the LFP cathode plate. In a similar way, the $LiNi_{0.6}Co_{0.2}Mn_{0.2}O_2$ (NCM622, Beijing Easpring Material Technology Co., Ltd) cathode (on aluminium foil) and graphite anode (Tianjin City Gateway Power Industry Co., Ltd., on copper foil) were prepared. As for the electrolyte, it consisted of 1 M $LiPF_6$ lithium salt in hybrid solvent ethylene carbonate (EC)/dimethyl carbonate (DMC) (LB-301 electrolyte, 1: 1 vol, Zhangjiagang Guotaihuarong New Chemical Materials Co., Ltd). In the part of research to detect whether the modified separator releases phosphorus-containing substances into the electrolyte during the circulation process, lithium

bis(trifluoromethanesulfonimide) (LiTFSI) replaced $LiPF_6$ to make convenience for substance detection. By putting the separator between a cathode and a lithium-metal anode and adding electrolyte in a glove box (M. Braun GmbH) filled with argon gas, a lithium half-cell (2016 coin) was assembled. In the same way, graphite half-cells were assembled with a graphite working electrode and a lithium-metal counter electrode. For combustion and thermal stability test, the pouch cells were assembled in the glove box through a winding process with double-side coated electrodes wrapped inside separators in the stack order of separator, anode, separator, cathode, separator, anode, separator and so on, then the electrolyte injecting and heat-sealing in the argon atmosphere were carried to produce the pouch cells.

2.4. Characterization and measurements

The bulk structure of the modified particles was characterized by X-ray diffraction (XRD, Rigaku, Japan), while the morphologies of modified particles, the surface and cross-section of different separators were investigated with a scanning electron microscopy (SEM, Hitachi, Japan) and a field emission scanning electron microscopy (FE-SEM, Zeiss, Germany). An EM TIC 3X triple ion-beam cutter (Leica, Germany) was used to cut the separator to obtain a flat cross-sectional surface. The chemical compositions of modified particles and separators were detected with an energy dispersive X-ray spectroscopy (EDS, Hitachi, Japan/Zeiss, Germany) and a Nicolet IS5 spectrometer (Thermo Fisher Scientific Inc.) in which the former made the elementary analysis and the later got Fourier transform infrared spectroscopy (FT-IR) in the range of 400–4000 cm^{-1}.

The fire resistance of the separators was studied by measuring the flame time of dry separators lit by fire. Then after adding 100 μL of LB-301 electrolyte and infiltrating every kind of separators, the wetted separators were lit by fire for 2 s to investigate the combustion phenomenon respectively.

Taking one measurement point every 10° Celsius from 110 °C to 200 °C, thermal shrinkage experiment of different separators were taken by clamping separators with two glass plates and storing at the certain temperature in a drying oven, and then the thermal shrinkage of separators was calculated according to the following equation:

$$\text{Thermal Shrinkage } (\%) = (S_0 - S) / S_0 \times 100\%$$

where S_0 and S mean the area of the separator before and after the heat treatment – after cropped to 2 cm square, with two glass plates clamped, storing at different temperatures for a certain time - respectively. At a heating rate of 5 °C min^{-1} from 25 °C to 600 °C, TG & DSC measurements were tested by a Model STA 449 instrument (NETZSCH Machinery and Instruments Co., Ltd).

For testing the flame resistance of pouch cells assembled by modified separators, NCM622 cathode (on aluminium foil) and graphite anode (on copper foil) were made into pieces. With a winding process, the pouches were then injected with the LB-301 electrolyte and heat sealed in a glove box (M. Braun GmbH). After 0.5C rate of a whole battery cycle, the outer packaging was removed and the inner part was directly lit by an open fire.

The electrolyte uptake (EU) of separators was calculated with this equation:

$$EU\ (\%) = (W - W_0) / W_0 \times 100\%$$

where W_0 and W are the weights of the separator before and after the soaking in the LB-301 electrolyte, respectively. Assuming that the volume occupied by hexadecane is equal to the porous volume, the porosity was calculated in a hexadecane an absorption process with the equation:

$$\text{Porosity } (\%) = (\Delta m / \rho) / V_0$$

where Δm is the change for mass of the separator between before and after the hexadecane absorption, ρ is the density of the hexadecane and V_0 is the total volume of the separator. The hydrophilic ability of surface were measured by contact angle with a contact angle goniometer (PowereachJC2000C1, Shanghai Zhongchen Digital Technique Equipment Co., Ltd). The Gurley value was measured by putting a piece of separator in an air permeability/porosity tester "Gurley" (4110 + 4320, Gurley, USA) and recording the reading after 100 mL of air passed. The ionic conductivity of separators was calculated by electrochemical impedance spectroscopy (EIS) using Autolab (Sino-Metrohm Technology Ltd) with a frequency range of 0.1–10^5 Hz, using the follow equation:

$$\sigma = L / (R_b \times A)$$

where σ is the ionic conductivity, L is the thickness of the separator, R_b is the bulk resistance obtained by the EIS test, and A is the area of the copper electrodes.

As for the electrochemical performance, the assembled 2016 coin batteries were load on a Neware battery program-control system in appropriate voltage range (LFP: 2.5–3.7 V; NCM622: 3.0–4.2 V; graphite: 0.005–3.0 V) with corresponding current rate for cycle performance testing and with 0.5C, 1C, 2C, 5C, 10C, 0.5C for rate performance testing, respectively. The Li/separator/stainless steel semi-blocking cell was assembled with fixture then the electrochemical stability window of different separators soaked in electrolyte was investigated by linear sweep voltammetry (LSV) on CHI660E electrochemical workstation (Shanghai Chenhua Instruments Limited) from 3 V to 6 V with the scan rate of 5 mV s^{-1}. In the semi-blocking battery, the reference electrode and the auxiliary electrode is a lithium sheet, and the working electrode is a stainless steel sheet.

For the batteries assembled with modified separators and DMVP additive, FE-SEM and EDS (Zeiss, Germany) were used to investigate the change of the graphite anode, and with a typical external standard method, ^{31}P NMR (500 MHz, Bruker, USA) was used to find the differences between different kinds of electrolyte.

3. Results and discussion

Many measurements were carried out to characterize the properties of modified particles, ensuring the process of silica formation and modification as described. The morphology of particles synthesized by the reverse microemulsion method was presented in the FE-SEM images of SiO_2 Fig. 2a and b. In the FE-SEM images, the KH570 modified SiO_2 particles have the uniform spherical shapes with an average diameter of about 33 nm, and after the reaction with DMVP, the average diameter increased to 42 nm, as the fitting results presented in Fig. S1a. Stated in the literature, the average diameter of MoO_3/SiO_2 nanocomposites synthesized by a typical reverse microemulsion method was about 23 nm [49]. Compared with the MoO_3/SiO_2 nanocomposites in the literature, in view of the usage of additional silane coupling agent in our synthesis process, the difference in particle size is reasonable. In addition, considering the reaction characteristics of phosphate [51], since the particles have been washed by toluene, the increase of the particle size from 33 nm to 42 nm could attribute to the double bond polymerization of KH570 and DMVP.

The energy dispersive X-ray spectroscopy (EDS) in Fig. 2c and Fig. S1b was get by choosing a low magnification image of DMVP modified SiO_2 ($mSiO_2$) particles and analyzing, which provides more information about element distribution. Since during sample preparation a silicon wafer was used as a substrate, the dark region in Si mapping belongs to silicon oxide, and the bright region corresponds to the silicon wafer substrate because of a higher Si content of substrate. The bright region in O mapping and P mapping seems analogous, corresponding to the dark region in Si mapping, which means that DMVP is grafted onto the resulting product modified particles. Besides, by comparing the weight after DMVP grafting reaction with the weight before the reaction, a mass increase of about 10% can be obtained,

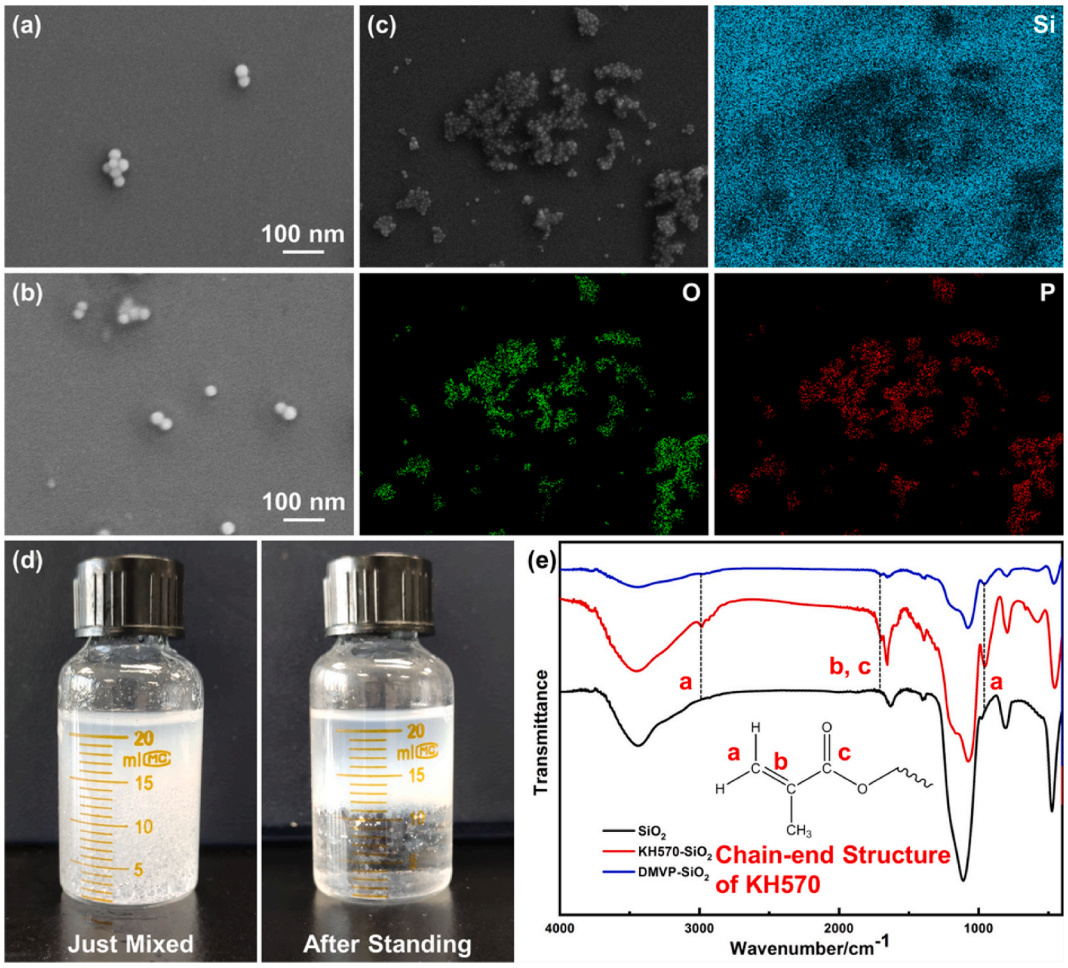

Fig. 2. Characterizations of modified particles: (a, b) FE-SEM images of KH570 modified SiO_2 and $mSiO_2$; (c) EDS spectra of $mSiO_2$; (d) experiment of hydrophilicity and lipophilicity of $mSiO_2$; (e) FT-IR of normal SiO_2, KH570 modified SiO_2 and $mSiO_2$.

which is close to the amount calculate by the element ratio of O and P.

Regarding the bulk structure of the product, in the result of X-ray diffraction (XRD) in Fig. S1c, the broad peak at 22° coincided with the characteristic peak of amorphous silica, which proves that the amorphous silica powder material was indeed synthesized through the reverse microemulsion method [52]. In addition, there was no other peak in the diffraction result, indicating that there was no crystalline impurity during the synthesis process.

In order to visually show the results of the grafting reaction, in the experiments based on hydrophilicity and lipophilicity of modified particles shown in Fig. 2d and Fig. S1d [53]. When it is placed in a mixed solvent of water and toluene, usually The SiO_2 particles tend to be dispersed in water, while the modified particles tend to be dispersed in the oily solvent toluene.

More details are shown in FT-IR characterization in Fig. 2e, compared with normal SiO_2, the peak at about 1700 cm^{-1} could be observed after KH570 modified due to the C═O bond stretching vibration in the chain structure of KH570. Besides, a peak appears at about 1680 cm^{-1}, which is the stretching vibration of the C═C bond, indicating that the existence of C═C bond after reaction. For DMVP modified process, Fig. 2e implies the decrease of the peak at 2700–2900 cm^{-1} which means the C–H bending vibration in the C═C bond of the chain end. Moreover, compared with the broad peak of –OH at 3500 cm^{-1}, the C–H formation vibration at about 900 cm^{-1} seems to increase first and then relatively decrease, corresponding to the double bond component first increasing and then decreasing. It implies the double bond reaction of KH570. After the reaction of DMVP, the bending vibration and vibration formation of C–H can still be observed, which indicates that there is still a segment of double bond from the graft. Considering the weight increase is about 10% after reaction, it is considered reasonable that some double bonds in the chain structure of KH570 are not reacted.

Fig. 3a and b presents the photographic image of the normal SiO_2 particles coated PE (PE-nSiO_2) separator and the DMVP modified SiO_2 particles coated PE (PE-mSiO_2) separator. Because of the same production process and the similar visible appearance of particles, these two images seem similar. On the surface of membrane, the silica nanoparticles are neatly arranged. After pre-treated by Leica EM TIC 3X triple ion-beam cutter, in the cross-sectional morphologies shown in Fig. 3c and d, the ceramic coating layer is brighter than the part of PE separator, and could be measured by the method of proportional zoom, coming to conclusion that the thickness of layer is about 3.5 μm.

The EDS spectra in Fig. 3e contained more information about PE-mSiO_2 separator itself and the DMVP grafting process. While elemental C is distributed homogeneously throughout the cross-section, the distribution of element Si and P is closely related to coating structure. On the ceramic coating, the elements Si and P are distributed in a large amount, away from the ceramic coating, the content of the element Si and P is almost zero. This phenomenon indicates that the coating is rich in Si and P element, implying the success of the DMVP grafting reaction.

As we know, separators must be chemically stable, thermally stable and mechanically stable to directly separate the cathode and anode electrodes. However, the widely used PE separators have a melting point of about 135 °C, which is obviously lower for thermal runaway situations. Ceramic layer could help PE separator keep its own shape in high

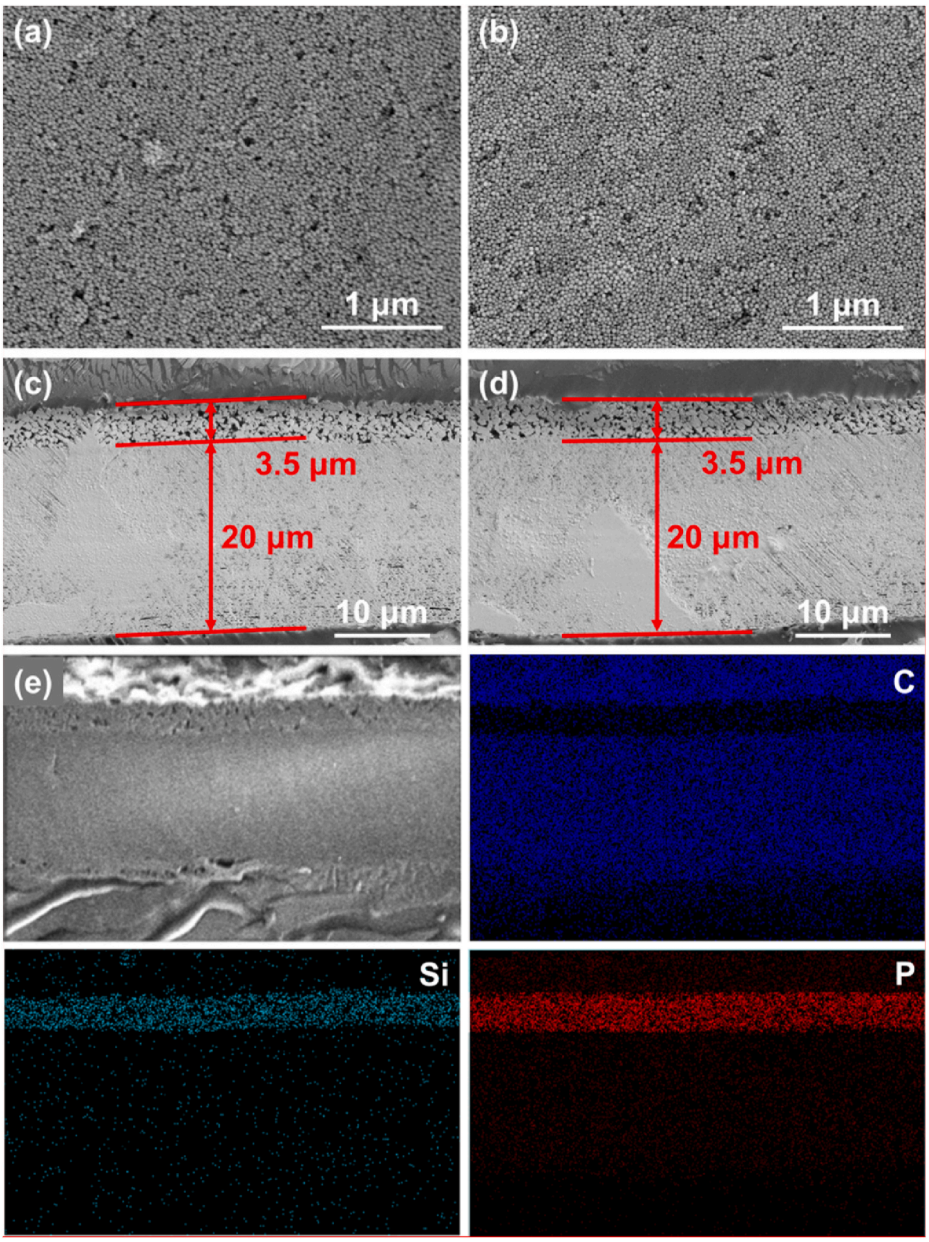

Fig. 3. Characterizations of different separators: (a, b) surface SEM images of PE-nSiO_2 and PE-mSiO_2; (c, d) cross-sectional FE-SEM images of PE-nSiO_2 and PE-mSiO_2; (e) EDS spectra of PE-mSiO_2.

temperature situation, but the extent of improvement is also limited. As for PE-mSiO_2 in this research, due to its more uniform ceramic coating layer and ability of releasing phosphorus free radicals at a high temperature, the improvement in thermal stability is more obvious. By putting separators sandwiched between two glasses in a drying oven and then setting different temperatures and holding for 30 min, the thermal shrinkage is directly observed and the thermal stability of separators is qualitatively measured. In Fig. 4a and Fig. S2, the bare commercial PE separator obviously melts at 130 °C and folds into one piece at 150 °C. When ordinary SiO_2 particles are coated, the PE-nSiO_2 separator begins to fold and deform at 160 °C, but cannot maintain its own shape at 180 °C. At the same time, when the DMVP-modified SiO_2 particles are coated, the PE-mSiO_2 membrane starts to melt slightly at 150 °C and has a basic shape at 200 °C. The results show that the DMVP modification enhances the heat resistance of the PE separator, showing that it is more difficult to shrink.

Besides, the microscopic appearances of heat-treated separators under the electron microscope also provide some other clues. After 150 °C heat treatment, the PE-nSiO_2 separator could maintain its dimensional stability visible to the naked eyes. However, the cracking of the ceramic layer occurred on the microscopic scale in Fig. 4c, which means an unstable structure that will collapse completely. Different from that situation, in Fig. 4d, after 200 °C heat treatment, the ceramic layer of PE-mSiO_2 separator is intact without any crack, which leads to a thermal stable structure. To explain the phenomenon, thermal gravimetric tests were carried at a heating rate of 5 °C·min^{-1} under Ar atmosphere. In the TG and DSC results under Ar atmosphere (Fig. 4e), the endothermic peaks at about 135 °C correspond to the melting process of PE, and the other endothermic peaks between 400 and 500 °C correspond to vaporization of organic components. It is worth noting that there is a wide peak between 150 and 200 °C for PE-mSiO_2 that cannot be attributed to a phase transition process, considering the fact that melting temperature of phosphorous polymers is higher than this range. Actually, it can be classified as the heat released by the reaction of

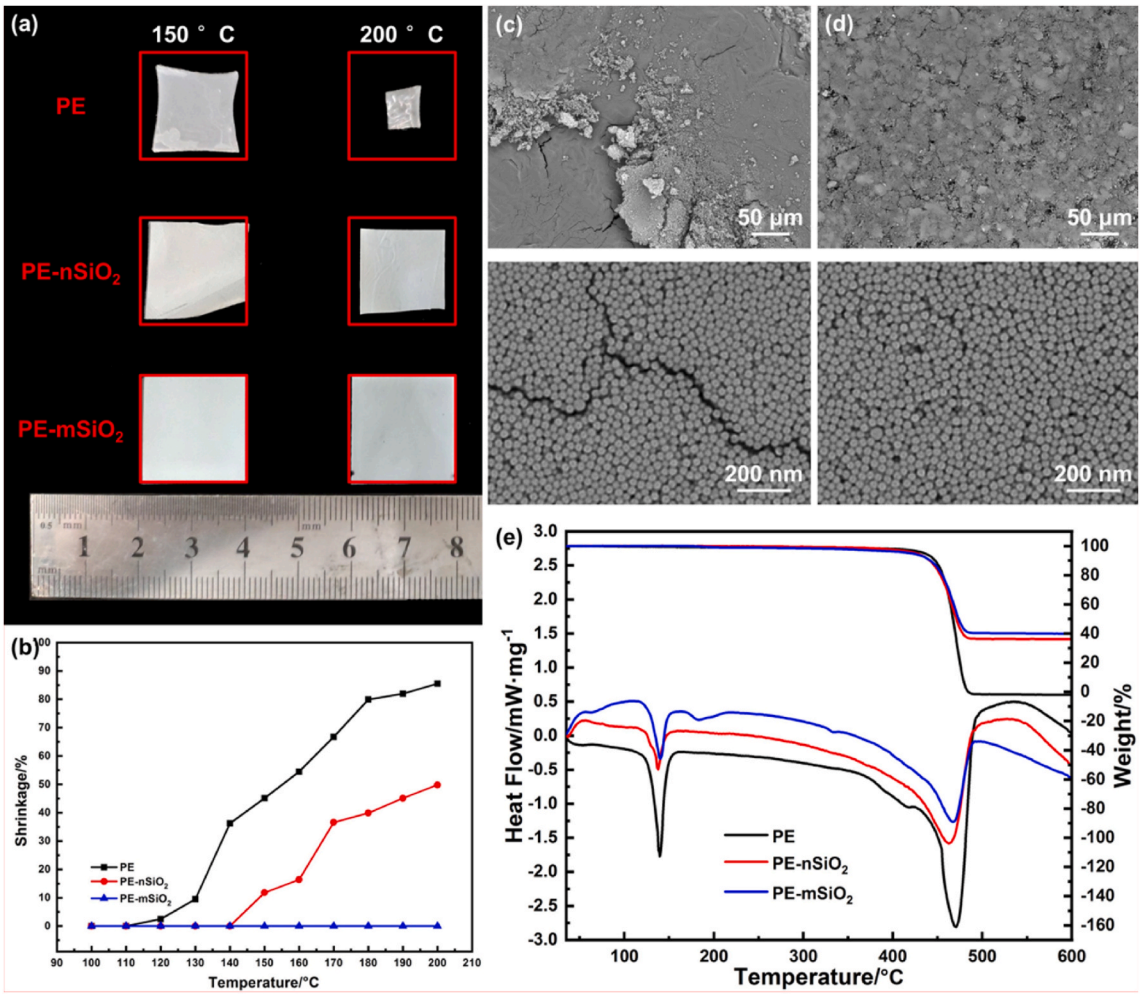

Fig. 4. Thermal shrinkage experiment of different separators: (a, b) thermal shrinkage of PE, PE-nSiO$_2$ and PE-mSiO$_2$; (c, d) surface SEM images of PE-nSiO$_2$ and PE-mSiO$_2$ after heat treatment; (e) DSC and TG results at a heating rate of 5 °C·min^{-1} under Ar atmosphere.

releasing phosphorus free radicals from polymerized DMVP after heating. Therefore, the heating condition of the ceramic layer was changed, and the ceramic would not directly crack [54–56]. We speculate that relatively high temperature between 150 and 200 °C can provide an effect similar to calcination, thereby strengthening the ceramic layer and maintaining dimensional stability to a certain extent [33]. These facts showed that the DMVP modified particles could maintain its status at higher temperature and significantly enhance the thermal stability.

Except the thermal shrinkage, the fire resistance is another effective measurement method of the safety performance of separators. Shown as Fig. S3, when the dry separator is placed near an open flame, the bare PE separator immediately shrinks and burns violently, while the PE-mSiO$_2$ separator has its own shape without any shrinkage, and the subsequent shrinking process also shows a significant difference. When a wet separator soaked by electrolyte tested in a similar method, good results are also obtained in the test. In Fig. 5 and Fig. S4, every kind of separators was lit by fire for 2 s after adding 100 μL of electrolyte and infiltrating. It could be seen that the bare PE separator and the PE-nSiO$_2$ separator kept burning after open fire source removed. PE-nSiO$_2$ separator burned for 23 s, showing a slightly better contraction behavior than the bare PE separator due to the existence of relatively stable ceramic layer. The PE-mSiO$_2$ shows similar contraction behavior to the DMVP added PE-nSiO$_2$ separator, which could be understood that the fixed DMVP could be decomposed to phosphorus free radicals when the PE-mSiO$_2$ separator is heated, thus phosphorus ingredients play the role of the flame retardant [43–45]. In the 2 s ignition time, the chain reaction of hydrogen and oxygen free radicals is interfered effectively, manifested as the macroscopic combustion reaction is prevented. After removing the open fire, the separator is rapidly cooled down, leading to the maintained morphology without any shrinkage in visual observation. In subsequent experiments, after increasing the ignition time, the separator could no longer maintain its morphology. This is due to the fact that the effective flame-retardant ingredients are exhausted during the ignition process, and because the phosphorus compound is not infinite, a burning phenomenon occurs [35].

The tests above are just related to the separators themselves, the doubt still existed whether the PE-mSiO$_2$ separator would take effect in a battery system. So NCM622 cathode (on aluminum foil), graphite anode (on copper foil), different separators and LB-301 electrolyte are used to assemble pouch cells to investigate the thermal runaway situation. After a whole battery cycle, the pouch cells are charged to fully charged state at which batteries contained enough energy and had higher risk when a thermal runaway occurred. Then the aluminum plastic films are quickly stripped and the inner part, cathode and anode twined with separator and soaked with electrolyte, is immediately lit by open fire for 2 s. Taken by our camera, there is no very obvious difference between the shrinkage behaviors of the bare PE separator and PE-nSiO$_2$ separator. These two kinds of separators are lit rapidly and fire burned violently, then the flame became smaller and finally extinguished at about 30 s. The difference is that for the bare PE separator, more active materials felled off from the cathode and anode. For the DMVP added pouch cells, it does not burn at all within the 2 s ignition time due to the function of

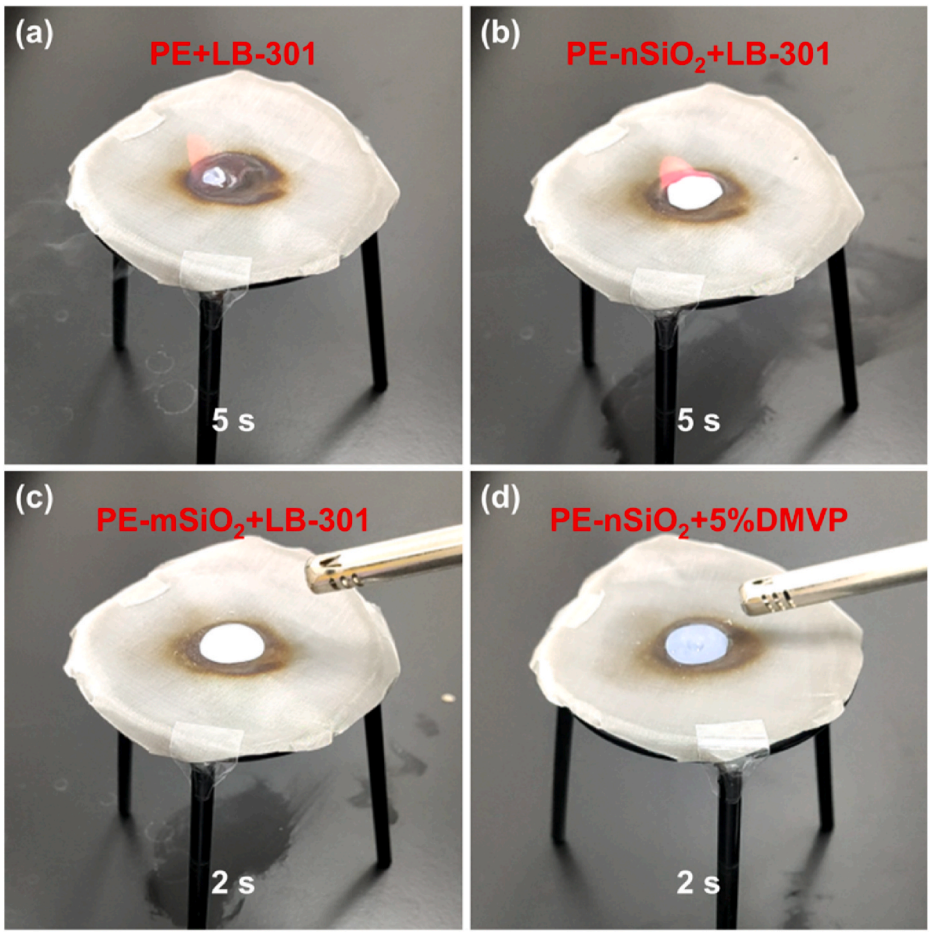

Fig. 5. Ignition experiment of different wet separators: (a) bare PE separator, adding LB-301 electrolyte; (b) PE-nSiO_2, adding LB-301 electrolyte; (c) PE-mSiO_2, adding LB-301 electrolyte; (d) PE-nSiO_2, adding the electrolyte containing 95% of LB-301 and 5% of DMVP (by weight).

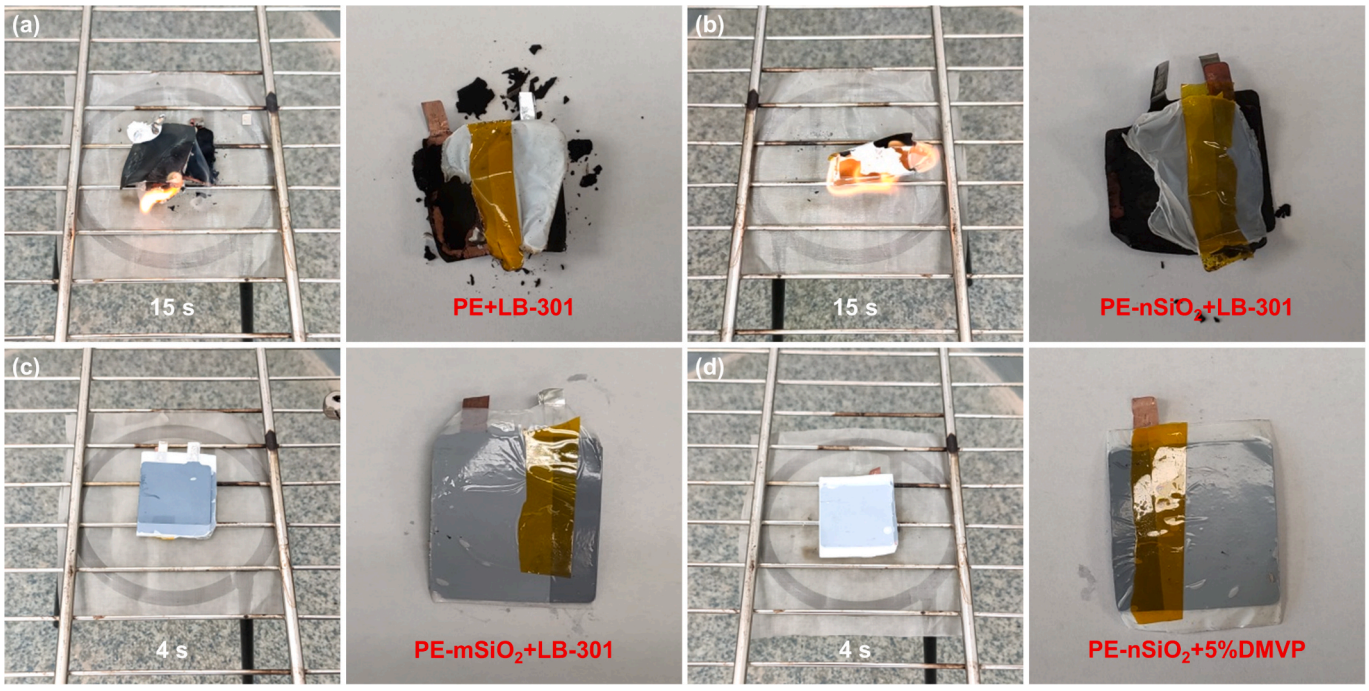

Fig. 6. Ignition experiment of pouch cells using different separators: (a) bare PE separator, adding LB-301 electrolyte; (b) PE-nSiO_2, adding LB-301 electrolyte; (c) PE-mSiO_2, adding LB-301 electrolyte; (d) PE-nSiO_2, adding the electrolyte containing 95% of LB-301 and 5% of DMVP (by weight).

DMVP as flame retardant [43–45]. The key is that the use of PE-mSiO$_2$ diaphragm will burn, but the fire is very small, and it is quickly extinguished. Unlike a wet separator, when assembling the soft pack battery, more amount of electrolyte was used, this is a combustible material that cannot be ignored and the DMVP fixed on the separator could not directly play the role of flame retardant. After ignition, the PE-mSiO$_2$ partition prevents further combustion, and the free phosphorus radicals released make the flame extinguish. As shown in Fig. 6 and Fig. S5, the partition slightly shrinks, but does not burn violently. The experiments above show that the PE-mSiO$_2$ separator is helpful to improve the safety

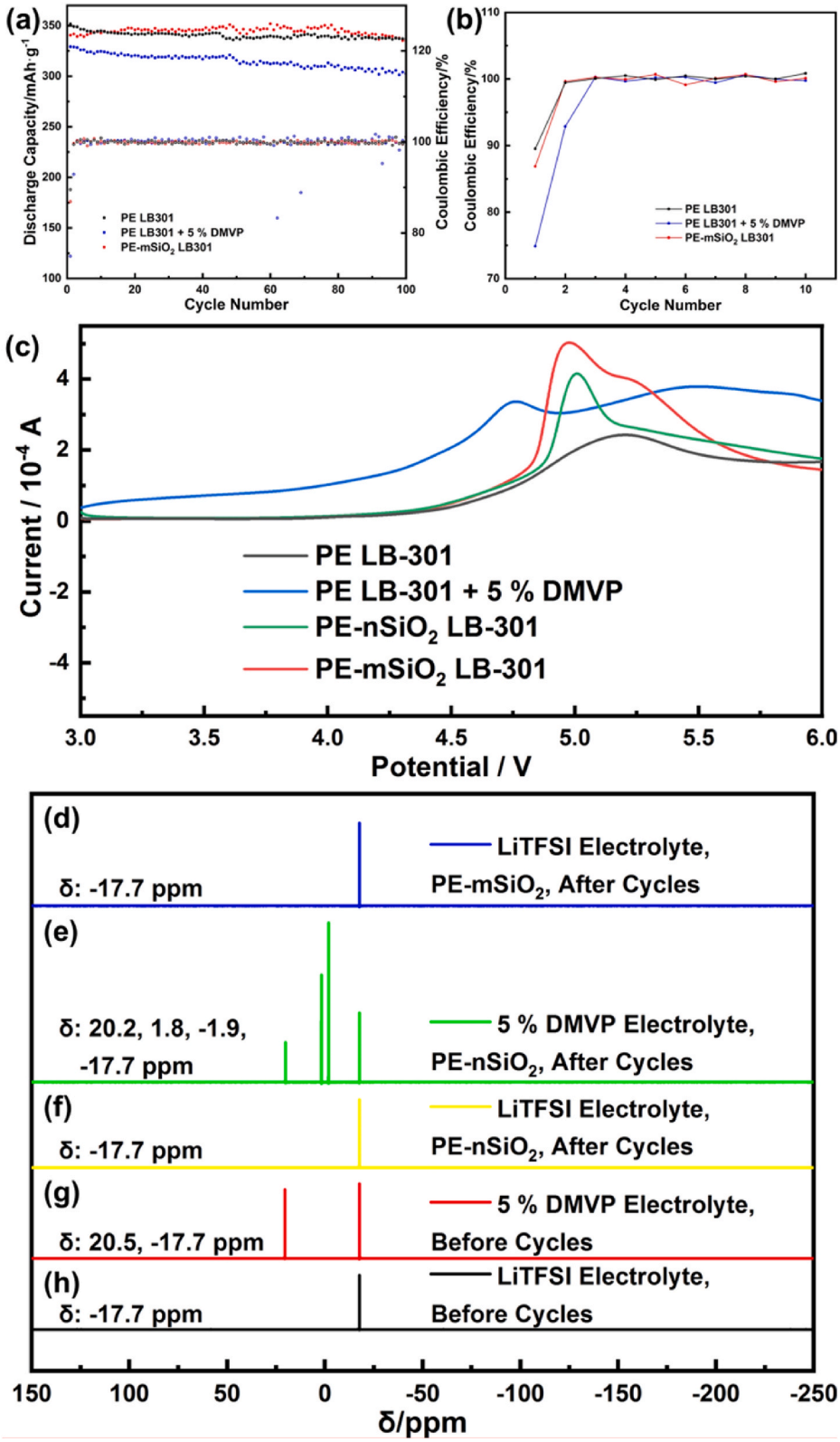

Fig. 7. (a, b) Cycle performance of graphite half-cells assembled with the DMVP additive, the PE-nSiO$_2$ and PE-mSiO$_2$; (c) LSV curves of different separators soaked in different LB-301 electrolyte; (d–h) ^{31}P NMR spectroscopy of different LiTFSI electrolytes.

at high temperature whether it is dry separator, wet separator or actual battery system.

Besides, bare PE separators are not completely capable with conventional liquid electrolytes due to its lyophobic features, such as a relatively low surface energy, which is harmful to power performance and cycle lives of LIBs. By using ceramic coating, this problem can be overcome. The relevant contact angle test is shown in Fig. S6. For a bare PE separator, the contact angle is about 46°, while for a PE-nSiO_2 separator the number decreases to nearly 15°. Considering the introduction of organic DMVP component, the PE-mSiO_2 separator would be more lyophilic to organic electrolytes, and its contact angle is about 10°. Then the electrolyte uptake amounts of three types of separators are tested for quantitative measurement, the result is shown as Table S1. The increase in hydrophilic property could indeed improve the liquid retention capacity of the separator, resulted in a better ionic conductivity and cycle stability [33]. The Gurley values and the porosity of ceramic separator are within the normal range, proving that our coating method is reliable.

Different separators were used for the assembly of LFP half-cells, NCM622 half-cells and graphite half-cells, and the battery cycle performances are shown in Fig. S7 and Fig. 7.

In the LFP half-cells using PE-mSiO_2 separators with the C-rate of 0.5, the discharge capacity of 1st cycle is 145.3 mAh g^{-1}, and it could maintain a capacity closed to 130 mAh g^{-1} after 400 cycles which is not significantly different from that of normal LFP half-cells. As for its rate performance, similar to PE-nSiO_2 separator, due to the better electrolyte uptake of the ceramic layer, it would be slightly better than a LFP half-cell using bare PE separator.

In the NCM622 half-cells with the C-rate of 0.5, the capacity fading in 100 cycles of the battery using PE-mSiO_2 separator and self-prepared reference LB-301 electrolyte is about 10 mAh g^{-1}, similar to the number of PE-nSiO_2 separator and self-prepared reference electrolyte, while the capacity fading is about 18 mAh g^{-1} when using PE-nSiO_2 separator and adding 5 wt % DMVP as additive. It attributed to the side effect of additive DMVP, as the literature discovered [46,47]. In the PE-mSiO_2 separator, the component of DMVP is held on the membrane, so it would not do harm to the battery cycles.

In the lithium-graphite half-cells with the C-rate of 0.2, the phenomenon is more obvious [57]. Except for the first two cycles, the Coulombic efficiencies batteries were basically close to 100%. The first cycle Coulombic efficiency of the battery using PE-nSiO_2 separator and reference LB-301 electrolyte is 84.5%, the specific capacity after activation is about 350 mAh g^{-1}; for the battery using PE-mSiO_2 separator and self-prepared reference electrolyte, these two amounts stayed 81.9% and 356 mAh g^{-1}. However, when using PE-nSiO_2 separator and adding 5 wt % DMVP as additive, the specific capacity dropped to 289 mAh g^{-1} and the first cycle Coulombic efficiency was just 74.8%. For the graphite half-cells at 60 °C with the C-rate of 0.5, there is no obvious difference between the performance of the battery using PE-mSiO_2 separator and that of the battery using bare PE-nSiO_2 separator. The first cycle Coulombic efficiencies are 91.3% and 89.8%, and the specific capacities remains stable in 50 cycles. Compared with the situation using of DMVP additive, when PE-mSiO_2 separator was used, DMVP is fixed on the separator by chemical interactions, which would not negatively affect specific capacity and first cycle Coulombic efficiency.

Shown in Fig. 7 and Fig. S7, to prove that the DMVP is fixed on a PE-mSiO_2 separator, LSV curves of different separators soaked in LB-301 electrolyte were provided, and ^{31}P NMR spectroscopy was tested by replacing the lithium salt $LiPF_6$ with LiTFSI and repeating the battery cycling process [58,59].

The LSV curve illustrates the existence of DMVP from the perspective of the electrochemical reaction process of the separator. As we known, the PE separator itself is relatively stable up to 6 V vs Li/Li^+, and the LSV curves of bare PE had only one oxidation peak at about 5.2 V, which could be attributed to the decomposition of $LiPF_6$ and solvent. When additive DMVP added to the electrolyte, a new peak appeared at about 4.8 V, which corresponds to the oxidation of free DMVP. For ceramic separator PE-nSiO_2 and PE-mSiO_2, the peak for the decomposition of $LiPF_6$ and solvent was about 5 V, and there was no peak for free DMVP oxidation. For the peak displacement, it could be understood as the difference in liquid retention capacity for ceramic and bare PE separator; and for the PE-mSiO_2, the absence of peak at about 4.8 V proved the existence of firm immobilization of DMVP from the side. To conclude, the LSV curves prove to a certain extent that DMVP is firmly fixed and the separator is electrochemical stable.

Correspondingly, the ^{31}P NMR spectroscopy explains the existence of DMVP from the perspective of the results of different reactions. Since the electrolyte content in the button battery decreases rapidly after the battery is cycled, the composition is more complicated, and the direct addition of deuterated solvents and phosphorus-containing standard materials may affect the measurement, so the experimental design of the external standard method is adopted, shown in Fig. S7. Various electrolytes were directly encapsulated in capillary tubes, and then standard substance solutions prepared from triphenyl phosphate solute and deuterated chloroform solvent at a ratio of 30 mg solute per 1 mL solvent were added to the NMR tube. Finally, putting the capillary into the NMR tube not only reduces the contact between the electrolyte and the air, but also avoids the influence of standard substances and deuterated solvents on the measurement, and also reduces the amount of electrolyte required. It has been reported in the literature that the chemical shift of the standard substance triphenyl phosphate is −17.7 ppm, which is consistent with our measurement results [59,60]. In the electrolyte with only LiTFSI as the lithium salt, no other peaks existed before and after battery cycles. After adding 5% of DMVP, a chemical shift of 20.5 ppm appears, which is proved to be the characteristic chemical shift of phosphorus in DMVP. After the electrochemical process, the characteristic chemical shift of DMVP still exists, and chemical shift peaks of 1.8 and −1.9 ppm also appears. These two transitions indicate the presence of the unsaturated bond reaction of DMVP, which is consistent with the behavior of inserting graphite anodes during cycling. When using a PE-mSiO_2 separator, the chemical shift after cycling is the same as that of the electrolyte with LiTFSI as the lithium salt, and there is no other phosphorus-containing component peak. At a relatively high temperature 60 °C, this phenomenon is also present in ^{31}P NMR spectroscopy of electrolyte after battery cycle, as shown in Fig. S7. At this time, DMVP is not free in the liquid phase and does not participate in the chemical reaction in the electrolyte, even in a higher temperature 60 °C. Considering the sensitivity of NMR to trace P species, the fact indicates that the chemical interaction firmly fixes the DMVP on the PE-mSiO_2 separator.

In order to know the specific reasons for the capacity loss of the graphite anode, the batteries cycling with LiTFSI electrolyte were disassembled, then the graphite anode was cleaned with the solvent ethylene carbonate (EC) and dimethyl carbonate (DMC), dried and sampled, then used for FE-SEM images and EDS spectra [61,62]. In Fig. 8, before being used in any electrochemical process, graphite particles can be easily observed under an electron microscope. There is F element distribution in EDS spectra, due to PVDF binder containing F element is selected when preparing the anode electrode. After the battery cycle, the content of F element has increased, which is related to the LiF and other fluorine-containing components in the formed SEI. For the battery equipped with PE-nSiO_2 separator, the morphology of the graphite anode does not change much after the battery cycle, and it still maintains an obvious spherical shape. For batteries added DMVP additive, it was difficult to see the spherical shape of the graphite, and the surface of graphite became more uneven. In the EDS spectra, bright P element area could be observed, which is consistent with the DMVP additive embedded in the graphite anode in the previous literature [46,47,57]. For batteries using PE-mSiO_2 separator, DMVP is fixed on the membrane and does not participate in the relevant electrochemical process, so the morphology of graphite after the cycle is closer to the PE-nSiO_2 using situation, and the distribution of P element is not

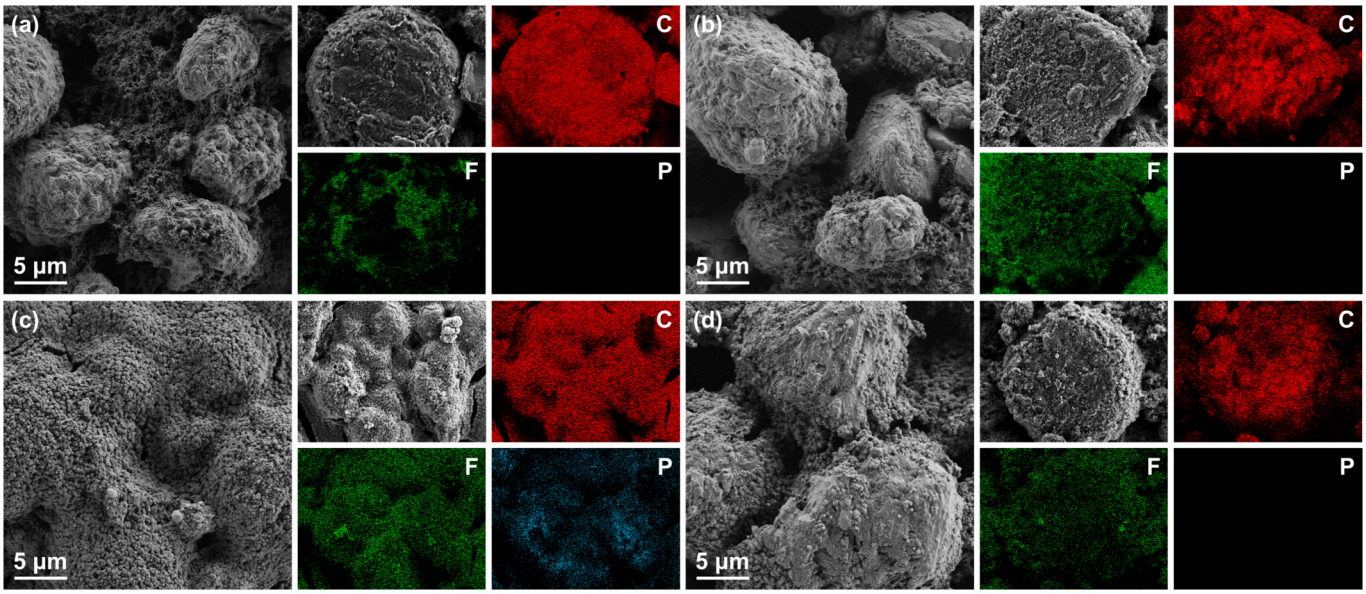

Fig. 8. FE-SEM images and EDS spectra of graphite anode: (a) without electrochemical process; (b) after 100 battery cycles with PE-nSiO_2 and LiTFSI electrolyte; (c) after 100 battery cycles with PE-nSiO_2, LiTFSI electrolyte and the DMVP additive; (d) after 100 battery cycles with PE-mSiO_2 and LiTFSI electrolyte.

observed in the EDS spectra. Combining the ^{31}P NMR results, it can be concluded that the reason for the capacity loss of the graphite anode during cycling is the embedding of the phosphate ester additives described in the literature [61,62]. And the above phenomenon will not occur if DMVP is fixed.

4. Conclusions

In this work, a technology that combines flame-retardant electrolyte additives with commercially available PE separators is used to effectively improve the battery safety. Through the reverse microemulsion method and simple coating process, organic phosphonate modified silica can be prepared and then coated on the bare PE separator. This technology retains the characteristics of ceramics and introduces the flame retardant properties of phosphonates, thereby enhancing the thermal stability of the separator. In addition, the phosphonate component is fixed on the separator, preventing side reactions between the phosphonate and commercial carbon anodes. Therefore, the battery assembled with the developed separator exhibits excellent safety performance and good electrochemical performance without irreversible capacity loss. Our research puts forward a new idea of using electrolyte additives in the field of diaphragms and also strengthens the widespread use of ceramic diaphragms.

Author contribution

Jinbao Zhao – Conceptualization, Methodology, Writing – Review & Editing, Supervision;

Peng Zhang – Conceptualization, Methodology, Writing – Review & Editing, Supervision;

Boyang Huang – Validation and Investigation (all parts), Formal analysis, Data Curation, Writing – Original Draft, Visualization;

Haiming Hua – Validation and Investigation (NMR part), Formal analysis, Writing – Review & Editing;

Longqing Peng – Validation and Investigation (thermal stability part);

Xin Wang – Validation and Investigation (ceramic coating part);

Xiu Shen – Writing – Review & Editing;

Ruiyang Li – Writing – Review & Editing.

Declaration of competing interest

The authors declare that they have no known competing financial interests or personal relationships that could have appeared to influence the work reported in this paper.

Acknowledgments

This work was financially supported by the National Natural Science Foundation of China (21875195, 22021001), National Key Research and Development Program of China (2017YFB0102000), Fundamental Research Funds for the Cornell University (20720190040), The Key Project of Science and Technology of Fujian Province (2018H6019) and The Key Project of Science and Technology of Xiamen (3502Z20201013).

Appendix A. Supplementary data

Supplementary data to this article can be found online at https://doi.org/10.1016/j.jpowsour.2021.229908.

References

[1] J.B. Goodenough, Y. Kim, Chem. Mater. 22 (2010) 587–603.
[2] J.M. Tarascon, M. Armand, Nature 414 (2001) 359–367.
[3] M.M. Thackeray, C. Wolverton, E.D. Isaacs, Energy Environ. Sci. 5 (2012).
[4] Q. Wang, P. Ping, X. Zhao, G. Chu, J. Sun, C. Chen, J. Power Sources 208 (2012) 210–224.
[5] X. Feng, D. Ren, X. He, M. Ouyang, Joule 4 (2020) 743–770.
[6] A.R. Baird, E.J. Archibald, K.C. Marr, O.A. Ezekoye, J. Power Sources 446 (2020).
[7] X. Huang, J. Solid State Electrochem. 15 (2010) 649–662.
[8] V. Deimede, C. Elmasides, Energy Technol. 3 (2015) 453–468.
[9] C. Martinez-Cisneros, C. Antonelli, B. Levenfeld, A. Varez, J.Y. Sanchez, Electrochim. Acta 216 (2016) 68–78.
[10] C. Yuan, L. Wang, S. Yin, J. Xu, J. Power Sources 467 (2020).
[11] A. Mauger, C.M. Julien, J.B. Goodenough, K. Zaghib, J. Electrochem. Soc. 167 (2020).
[12] J. Zhang, J. Zhao, L. Yue, Q. Wang, J. Chai, Z. Liu, X. Zhou, H. Li, Y. Guo, G. Cui, L. Chen, Adv. Energy Mater. 5 (2015).
[13] S.Y. Xiao, Y.Q. Yang, M.X. Li, F.X. Wang, Z. Chang, Y.P. Wu, X. Liu, J. Power Sources 270 (2014) 53–58.
[14] X. Shen, H.M. Hua, H. Li, R.Y. Li, T.X. Hu, D.Z. Wu, P. Zhang, J.B. Zhao, Polymer (2020) 201.
[15] D. Wang, J.-Q. Zhang, L.-L. Liu, M.-Z. An, P.-X. Yang, X.-N. Pan, Y. Li, Z.-P. Wang, 26 (2020) 406-412.
[16] Y. Shen, Y. Zhang, S. Han, J. Wang, Z. Peng, L. Chen, Joule 2 (2018) 1674–1689.

[17] J.R. Nair, L. Imholt, G. Brunklaus, M. Winter, Electrochem. Soc. Interface 28 (2019) 55–61.
[18] H.-S. Jeong, D.-W. Kim, Y.U. Jeong, S.-Y. Lee, J. Power Sources 195 (2010) 6116–6121.
[19] W.-K. Shin, D.-W. Kim, J. Power Sources 226 (2013) 54–60.
[20] C. Shi, P. Zhang, L. Chen, P. Yang, J. Zhao, J. Power Sources 270 (2014) 547–553.
[21] H. Huo, X. Li, Y. Chen, J. Liang, S. Deng, X. Gao, K. Doyle-Davis, R. Li, X. Guo, Y. Shen, C.-W. Nan, X. Sun, Energy Storage Mater. 29 (2020) 361–366.
[22] M.-H. Ryou, D.J. Lee, J.-N. Lee, Y.M. Lee, J.-K. Park, J.W. Choi, Adv. Energy Mater. 2 (2012) 645–650.
[23] R. Pan, X. Xu, R. Sun, Z. Wang, J. Lindh, K. Edstrom, M. Stromme, L. Nyholm, Small 14 (2018), e1704371.
[24] X. Chen, R. Zhang, R. Zhao, X. Qi, K. Li, Q. Sun, M. Ma, L. Qie, Y. Huang, Energy Storage Mater. 31 (2020) 181–186.
[25] C. Zhang, L. Shen, J. Shen, F. Liu, G. Chen, R. Tao, S. Ma, Y. Peng, Y. Lu, Adv. Mater. 31 (2019), e1808338.
[26] Y. Yang, W. Wang, J. Zhang, Mater. Today Energy 16 (2020).
[27] Z. Liu, Q. Hu, S. Guo, L. Yu, X. Hu, Adv. Mater. (2021), e2008088.
[28] Y.-T. Zhou, J. Yang, H.-Q. Liang, J.-K. Pi, C. Zhang, Z.-K. Xu, Compos. Commun. 8 (2018) 46–51.
[29] Y.S. Jung, A.S. Cavanagh, L. Gedvilas, N.E. Widjonarko, I.D. Scott, S.-H. Lee, G.-H. Kim, S.M. George, A.C. Dillon, Adv. Energy Mater. 2 (2012) 1022–1027.
[30] S.H. Lee, J. Kim, B.H. Kim, S. Yoon, K.Y. Cho, Small 15 (2019), e1804980.
[31] P. Yang, P. Zhang, C. Shi, L. Chen, J. Dai, J. Zhao, J. Membr. Sci. 474 (2015) 148–155.
[32] C. Shi, J. Dai, X. Shen, L. Peng, C. Li, X. Wang, P. Zhang, J. Zhao, J. Membr. Sci. 517 (2016) 91–99.
[33] J. Dai, C. Shi, C. Li, X. Shen, L. Peng, D. Wu, D. Sun, P. Zhang, J. Zhao, Energy Environ. Sci. 9 (2016) 3252–3261.
[34] L. Peng, X. Shen, J. Dai, X. Wang, J. Zeng, B. Huang, H. Li, P. Zhang, J. Zhao, J. Electrochem. Soc. 166 (2019) A2111–A2120.
[35] L. Peng, X. Kong, H. Li, X. Wang, C. Shi, T. Hu, Y. Liu, P. Zhang, J. Zhao, Adv. Funct. Mater. 31 (10) (2021) 2008537.
[36] L. Peng, X. Wang, J. Dai, X. Shen, B. Huang, P. Zhang, J. Zhao, Mater. Chem. Front. 5 (4) (2021) 1884–1894.
[37] X. Shen, C. Li, C. Shi, C. Yang, L. Deng, W. Zhang, L. Peng, J. Dai, D. Wu, P. Zhang, J. Zhao, Appl. Surf. Sci. 441 (2018) 165–173.
[38] S.S. Zhang, J. Power Sources 162 (2006) 1379–1394.
[39] A.M. Haregewoin, A.S. Wotango, B.-J. Hwang, Energy Environ. Sci. 9 (2016) 1955–1988.
[40] R. Zhou, J. Huang, S. Lai, J. Li, F. Wang, Z. Chen, W. Lin, C. Li, J. Wang, J. Zhao, Sustain. Energy Fuels 2 (2018) 1481–1490.
[41] Y.E. Hyung, D.R. Vissers, K. Amine, J. Power Sources 119–121 (2003) 383–387.
[42] B. Wu, F. Pei, Y. Wu, R. Mao, X. Ai, H. Yang, Y. Cao, J. Power Sources 227 (2013) 106–110.
[43] H.F. Xiang, H.Y. Xu, Z.Z. Wang, C.H. Chen, J. Power Sources 173 (2007) 562–564.
[44] E.-G. Shim, T.-H. Nam, J.-G. Kim, H.-S. Kim, S.-I. Moon, J. Power Sources 172 (2007) 919–924.
[45] E.-G. Shim, T.-H. Nam, J.-G. Kim, H.-S. Kim, S.-I. Moon, J. Power Sources 175 (2008) 533–539.
[46] N. von Aspern, S. Röser, B. Rezaei Rad, P. Murmann, B. Streipert, X. Mönnighoff, S. D. Tillmann, M. Shevchuk, O. Stubbmann-Kazakova, G.-V. Röschenthaler, S. Nowak, M. Winter, I. Cekic-Laskovic, J. Fluor. Chem. 198 (2017) 24–33.
[47] L. Li, Y. Chen, L. Qian, B. Xu, W. Xi, J. Appl. Polym. Sci. 135 (2018).
[48] W. Xu, Z. Wang, L. Shi, Y. Ma, S. Yuan, L. Sun, Y. Zhao, M. Zhang, J. Zhu, ACS Appl. Mater. Interfaces 7 (2015) 20678–20686.
[49] J. Wang, X. Li, S. Zhang, R. Lu, Nanoscale 5 (2013) 4823–4828.
[50] X. Wang, H. Hua, L. Peng, B. Huang, P. Zhang, J. Zhao, Appl. Surf. Sci. 542 (2021).
[51] J. Zheng, Y. Zhao, X. Feng, W. Chen, Y. Zhao, J. Mater. Chem. 6 (2018) 6559–6564.
[52] H. Hamdan, M.N.M. Muhid, S. Endud, E. Listiorini, Z. Ramli, J. Non-Cryst. Solids 211 (1997) 126–131.
[53] R.Y. Hong, H.P. Fu, Y.J. Zhang, L. Liu, J. Wang, H.Z. Li, Y. Zheng, J. Appl. Polym. Sci. 105 (2007) 2176–2184.
[54] R.-J. Jeng, S.-M. Shau, J.-J. Lin, W.-C. Su, Y.-S. Chiu, Eur. Polym. J. 38 (2002) 683–693.
[55] C.H. Lin, C.C. Feng, T.Y. Hwang, Eur. Polym. J. 43 (2007) 725–742.
[56] L.-L. Wei, D.-Y. Wang, H.-B. Chen, L. Chen, X.-L. Wang, Y.-Z. Wang, Polym. Degrad. Stabil. 96 (2011) 1557–1561.
[57] X. Wang, E. Yasukawa, S. Kasuya, J. Electrochem. Soc. 148 (2001).
[58] N. Dupre, M. Cuisinier, D. Guyomard, Interface Mag. 20 (2011) 61–67.
[59] D.S. Hall, U. Werner-Zwanziger, J.R. Dahn, J. Electrochem. Soc. 164 (2017) A2171–A2175.
[60] K. Xu, M.S. Ding, S. Zhang, J.L. Allen, T.R. Jow, J. Electrochem. Soc. 149 (2002).
[61] S.J. An, J. Li, C. Daniel, D. Mohanty, S. Nagpure, D.L. Wood, Carbon 105 (2016) 52–76.
[62] Y. An, H. Fei, G. Zeng, L. Ci, B. Xi, S. Xiong, J. Feng, J.Power Sources 378 (2018) 66–72.